Cadmium–cysteine coordination in the BK inner pore region and its structural and functional implications

Yu Zhou[1], Xiao-Ming Xia, and Christopher J. Lingle[1]

Department of Anesthesiology, Washington University School of Medicine, St. Louis, MO 63110

Edited by Richard W. Aldrich, University of Texas, Austin, TX, and approved March 20, 2015 (received for review January 15, 2015)

To probe structure and gating-associated conformational changes in BK-type potassium (BK) channels, we examined consequences of Cd^{2+} coordination with cysteines introduced at two positions in the BK inner pore. At V319C, the equivalent of valine in the conserved Kv proline-valine-proline (PVP) motif, Cd^{2+} forms intrasubunit coordination with a native glutamate E321, which would place the side chains of V319C and E321 much closer together than observed in voltage-dependent K^+ (Kv) channel structures, requiring that the proline between V319C and E321 introduces a kink in the BK S6 inner helix sharper than that observed in Kv channel structures. At inner pore position A316C, Cd^{2+} binds with modest state dependence, suggesting the absence of an ion permeation gate at the cytosolic side of BK channel. These results highlight fundamental structural differences between BK and Kv channels in their inner pore region, which likely underlie differences in voltage-dependent gating between these channels.

K^+ channels | Cd^{2+} coordination | state dependence | BK channels | Slo1 channels

How transmembrane potential influences the opening and closing of ion channels, a process known as gating, is central to understanding how cellular excitability is regulated (1). For voltage-dependent K^+ (Kv) channels, functional (2–4) and crystallographic (5, 6) studies have led to a compelling model of gating. In this model there are two key elements, both of which arise from properties of the cytosolic end of Kv channels: a cytosolic ion permeation gate formed by an interlaced arrangement of S6 inner helices termed the bundle crossing (2, 3), and a kink produced by the conserved proline-valine-proline (PVP) motif (Fig. 1*A*, boxed residues) to allow the C terminus of Kv S6 to form extensive contact with the S4–S5 linker (5, 6). Thus, the outward movement of the voltage sensors (VSDs) induced by transmembrane depolarization is thought to be transmitted to S6 through the S4–S5 linker to open the cytosolic ion permeation gate (6–8), and this enables access of cytosolic K^+ ions to the Kv inner pore region.

Although this model is generally accepted for Kv channel gating, it is not clear to what extent it applies to other K^+ channels. For example, the large conductance, Ca^{2+}-activated K^+ (BK or Slo1) channel shares with Kv channels a similar set of four VSDs attached to a central pore and gate domain (PGD), such that both channels are voltage dependent (9). However, unlike that of Kv channels, the inner pore of a closed BK channels is accessible to large molecules such as quaternary ammonium (QA) blockers (10, 11) and methanethiosulfonate ethyltrimethylammonium (MTSET) (12), indicating that the cytosolic end of a closed BK channel cannot completely occlude K^+ flow; this indicates that a gate extracellular to that proposed for Kv channels is required to securely prevent K^+ flow in a closed BK channel. As a corollary, the underlying structural and conformational details required to couple VSD activation to channel opening may differ between BK and Kv channels.

To provide new insight into differences between BK and Kv in the inner pore region, we have probed the cadmium (Cd^{2+}) sensitivity of cysteine residues introduced in the BK S6 inner helix. Compared with cysteine modification by MTSET (12), Cd^{2+}–Cys coordination provides two potential advantages for investigation of BK channel gating. First, Cd^{2+} coordination can involve multiple residues with strict distance and geometric requirements. This potentially provides information about the relative position of coordinating residues in the BK inner pore region, thereby placing important structural constraints on BK S6. Second, the size of Cd^{2+} is closer to that of a K^+ ion compared with large probes such as QA blockers or MTSET; this allows a more accurate evaluation of whether there may be restriction to K^+ flow at the cytosolic end of BK channel. Despite the evidence that large molecules can access the BK inner cavity in closed states, gated access of intracellularly applied Shaker ball peptide indicates that conformational changes do occur at the cytosolic end of BK channels (13). Furthermore, our previous study showed that the open-state modification of BK inner pore cysteines by MTSET is approximately two orders of magnitude faster than that in closed states (12), although the state dependence is weaker than that observed in Shaker channels (3). It is therefore important to determine the extent to which the BK cytosolic side may restrict inner pore access of K^+ by using a probe similar in size to K^+.

Here we focus on two BK S6 residues, V319 and A316, which confer interesting sensitivity to Cd^{2+} on BK channels when replaced by cysteine. V319 is in register with Kv residues that contribute to the bundle crossing in Kv channels. The results reveal that Cd^{2+} coordination occurs between V319C and E321 in the same BK α-subunit, requiring that BK S6 adopts a novel kink at this level that is distinct from that in Kv channel structures. Furthermore, for A316C, which lines the BK inner pore, the Cd^{2+} coordination rate differs only modestly between open and closed states, suggesting there is no significant restriction of K^+ access to the BK inner cavity in both states.

Results

Cd^{2+} Markedly Changes BK Currents by Coordinating with Cysteines Introduced at Two Separate Inner Pore Positions. BK channels pose several challenges in the use of Cd^{2+} as a probe of potential coordinating positions in the S6 inner helix. First, Cd^{2+} at concentrations up to 100 μM activates BK through a high-affinity

Significance

The voltage- and Ca^{2+}-activated BK-type (BK) K^+ channels serve as a key regulator of electrical and Ca^{2+} signaling as well as a model system for studying allosteric regulation of protein. By examining Cd^{2+} coordination with cysteines placed in BK S6 inner helix, our work reveals a previously undefined structural feature in the BK S6 at a position critical for the coupling between voltage sensor activation and channel opening. In addition, we show that BK S6 does not form an ion permeation gate in its cytosolic end. These results define specific structural constraints in the BK inner pore region that differ from voltage-dependent K^+ (Kv) channels.

Author contributions: Y.Z. and C.J.L. designed research; Y.Z. and X.-M.X. performed research; Y.Z. and C.J.L. analyzed data; and Y.Z. and C.J.L. wrote the paper.

The authors declare no conflict of interest.

This article is a PNAS Direct Submission.

[1]To whom correspondence may be addressed. Email: zhouy@wustl.edu or clingle@morpheus.wustl.edu.

This article contains supporting information online at www.pnas.org/lookup/suppl/doi:10.1073/pnas.1500953112/-/DCSupplemental.

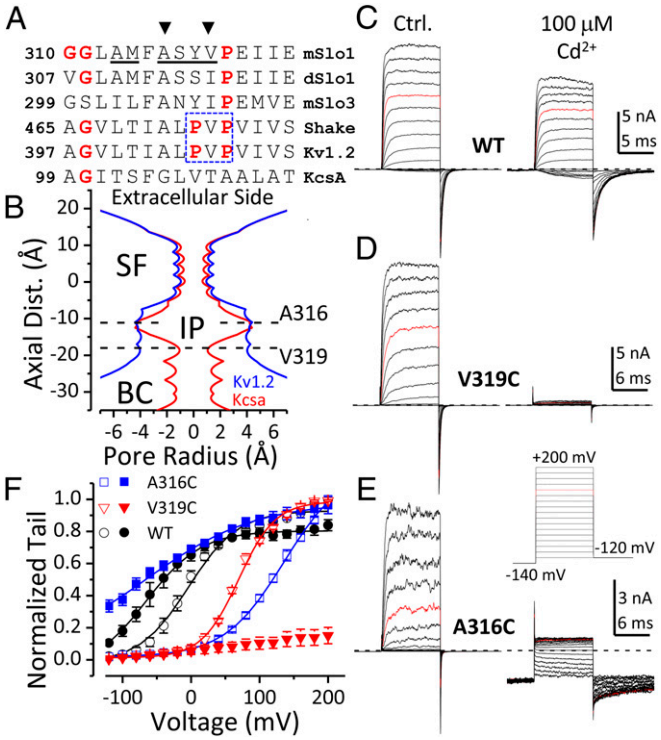

Fig. 1. Cd^{2+} coordinates with cysteines separately introduced at two BK inner pore sites. (*A*) Sequence alignment of the S6 segment in the inner pore regions of Slo family channels, Kv channels, and the KcsA channel. The conserved glycine hinge and prolines in the PVP motif (boxed residues) are colored in red. The sites evaluated with cysteine substitution in BK S6 are underlined. A316 and V319 are indicated by arrowheads. (*B*) Radius profiles of Kv1.2 (blue) and KcsA (red) channels calculated from their crystal structures. The approximate locations of A316C and V319C are marked by horizontal dotted lines. SF, selectivity filter; IP, inner pore; BC, bundle crossing. (*C–E*) Currents of WT, V319C, and A316C recorded in 300 μM Ca^{2+} without (*Left*) and with (*Right*) 100 μM intracellular Cd^{2+}. Voltage protocol was shown in *E*. (*F*) *G–V* relationships of WT (black circles), V319C (red triangles), and A316C (blue squares) in 300 μM Ca^{2+} without (open symbols) or with (filled symbols) 100 μM Cd^{2+}. Boltzmann fit results (lines) are $z = 1e$, $V_h = -3$ mV (WT, control); $z = 0.75e$, $V_h = -57$ mV (WT, Cd^{2+}); $z = 0.94e$, $V_h = +69$ mV (V319C, control); $z = 0.6e$, $V_h = +136$ mV (A316C, control); $z = 0.32e$, $V_h = -66$ mV (A316C, Cd^{2+}).

Ca^{2+}-sensing residue (D362) in the BK cytosolic domain (14, 15). Second, [Cd^{2+}] above 300 μM strongly blocks BK current with slow recovery (15). Therefore, the highest [Cd^{2+}] used in this study is 200 μM. In addition, to minimize Cd^{2+} effects on D362, all experiments were done in 300 μM Ca^{2+}. Under such conditions, 100 μM Cd^{2+} produces a leftward-gating shift of ~50 mV (Fig. 1*F*, circles), corresponding to a change in Gibbs free energy between closed and open states at 0 mV (ΔG_0) of −0.92 kcal/mol. In addition, the apparent maximal conductance is reduced (Fig. 1*C*), which we attribute to a direct fast channel blocking effect that can be discerned as a reduction in single-channel current amplitude. In construct E399A, a mutation that disrupts low-affinity divalent cation regulation of BK channels (16, 17), the Cd^{2+}-induced leftward-gating shift is changed to a 20-mV rightward-gating shift, with little effect on the fast channel block effect (Fig. S1). Based on these considerations, we have therefore focused on Cd^{2+} effects that are clearly distinguishable from background effects. Cd^{2+} sensitivity were examined in mutants with cysteine individually introduced from positions A313 through G327. At most positions, 100 μM intracellular Cd^{2+} produces effects that varied from the Cd^{2+} effect on WT channels by less than 1 kcal/mol (Fig. S2*M*).

Using Kv structures as a reference, in this study we focus on six BK-substituted positions aligning with those within or near the Kv inner pore region that are critical for Kv channel gating (Fig. 1*A*, underlined residues). For BK inner pore cysteine mutants A313C, M314C, S317C, and Y318C, the Cd^{2+}-induced changes in BK currents were either similar to that of WT channels or too weak to allow examination of state dependence (Fig. S2 *A–D*). For A316C and V319C, intracellular Cd^{2+} induces large (Fig. 1 *D* and *E*) but reversible (Fig. S3) changes in BK channel current properties.

The general features of Cd^{2+} action at V319C and A316C differ markedly. For V319C, the outward current is strongly inhibited by 100 μM intracellular Cd^{2+} (Fig. 1*D*). In contrast, at negative potentials when VSDs are largely inactive, the single-channel activity of V319C is not inhibited by intracellular Cd^{2+} (Fig. S4). For A316C, 100 μM intracellular Cd^{2+} negatively shifts the *G–V* relationship by more than 200 mV (Fig. 1*F*, blue squares). Coordination of Cd^{2+} with A316C also induces strong inhibition of outward current, probably resulting from the positive charges on Cd^{2+} that affect K^+ movement through the inner pore. Thus, Cd^{2+}-A316C coordination substantially increases BK current at negative potentials but reduces most outward current at positive potentials (Fig. 1*E*). Intriguingly, the effect of Cd^{2+}-A316C coordination on BK current is reminiscent of the phenotype of BK A316K or A316R mutants (18), which supports the idea that both the Cd^{2+}-induced gating shift and the Cd^{2+}-induced current inhibition arise from Cd^{2+}-A316C coordination.

It should be noted that cysteine mutants outside the BK inner pore, such as E321C and E324C, also exhibit Cd^{2+} sensitivity that is clearly distinct from WT (Fig. S2 *E* and *H*). Because the focus of this work is in the BK inner pore region, Cd^{2+} coordination in these mutants will not be considered further in this paper.

Cd^{2+} Coordination at V319C Involves a Native Glutamate E321 in the Same Subunit. The apparent Cd^{2+} affinity of V319C is ~20 μM (Fig. S5), which is comparable to the affinity of Cd^{2+} coordination sites formed by two Cd^{2+}-coordinating residues (19), including cysteine, histidine, aspartate, or glutamate (20). There are two native glutamates following the YVP motif in BK S6 (Fig. 1*A*; E321 and E324). To examine whether either of these residues participate in Cd^{2+}-V319C coordination, we individually mutated each glutamate to glutamine in the V319C construct and examined Cd^{2+} sensitivity of these mutants. Intracellular Cd^{2+} no longer coordinates with V319C to inhibit BK current when E321 is replaced by glutamine (Fig. 2*A*). However, Cd^{2+} inhibits V319CE324Q current with affinity similar to that of V319C (Fig. 2 *B* and *D*). The V319C in V319CE21Q can be modified by intracellularly applied MTSET (Fig. S6), indicating that V319C is still accessible in the V319CE321Q construct. Collectively, these results show that Cd^{2+} simultaneously coordinates with both V319C and E321; this is in contrast to Cd^{2+} coordination with Shaker V474C, which only involves C474 residues from neighboring subunits (3).

Next we asked whether V319C-Cd^{2+}-E321 coordination involves residues in the same subunit or from neighboring subunits. If the coordination involved an intersubunit metal bridge, coexpression of V319CE321Q with WT subunits should partially restore Cd^{2+} sensitivity. Contrary to this expectation, currents recorded from oocytes coinjected with V319CE321Q and WT RNAs are not inhibited by intracellular Cd^{2+} (Fig. 3 *A* and *B*), revealing that Cd^{2+} does not coordinate with V319C and E321 when they are not in the same subunit.

To verify that Cd^{2+} does not form an intersubunit bridge between V319C and E321, we examined single channels from oocytes coinjected with the V319CE321Q construct together with an Y294V construct. Y294V abolishes BK channel sensitivity to extracellular tetraethylammonium (TEA) (21). In the presence of extracellular TEA, the conductance of the resulting channel is determined by the number of Y294V subunits in the channel, thereby defining the stoichiometry of each channel from its

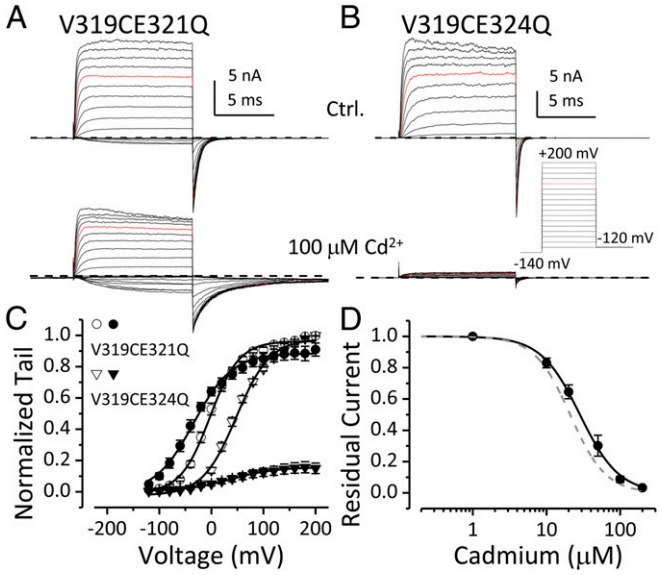

Fig. 2. Cd^{2+}-V319 coordination requires E321. (*A*) V319CE321Q currents without (*Upper*) and with (*Lower*) 100 μM intracellular Cd^{2+}. (*B*) V319CE324Q currents without (*Upper*) and with (*Lower*) 100 μM intracellular Cd^{2+}. Voltage protocol is shown. (*C*) *G–V* relationships of V319CE321Q (circle) and V319CE324Q (triangle) in 300 μM Ca^{2+} without (open symbols) or with (filled symbols) 100 μM Cd^{2+}. Boltzmann fit results (line) are $z = 0.9e$, $V_h = -3$ mV (V319CE321Q, control); $z = 0.7e$, $V_h = -35$ mV (V319CE321Q, Cd^{2+}); $z = 0.6e$, $V_h = 36$ mV (V319CE324Q, control). (*D*) Normalized residual BK current at +120 mV is plotted as a function of $[Cd^{2+}]_{in}$ for V319CE324Q channels. Hill function fit result (black line) is $IC_{50} = 28.4$ μM, $n = 1.6$. Gray dashed line represents Hill equation fit to $[Cd^{2+}]$-inhibition curve of V319C (Fig. S5; $IC_{50} = 21$ μM, $n = 1.8$).

single-channel current (22). Fig. 3*C* shows the single-channel activity of a homomeric BK channel formed by Y294VV319C subunits recorded at +70 mV. Extracellular TEA (1.5 mM) in the pipette solution did not block the channel, as expected (21, 22). Application of 100 μM $[Cd^{2+}]_{in}$ markedly reduced channel open probability (Po; red traces). The single-channel currents recorded from oocytes coinjected with V319CE321Q and Y294V in the presence of extracellular TEA (Fig. 3 *D1–D5*) revealed four distinct conductance classes indicative of four stoichiometric subunit combinations. However, none of these channels were inhibited by intracellular Cd^{2+}, suggesting that Cd^{2+} does not coordinate with V319C and E321 when they are in different subunits.

We also examined Cd^{2+} sensitivity of BK channels formed by Y294VV319C and E321Q subunits. The Po of the resulting channels was reduced by addition of intracellular Cd^{2+} (Fig. 3 *E1–E6*), but, importantly, the extent of Cd^{2+}-induced inhibition was dependent on the number of V319C subunits in the channel, with stronger inhibition in channels containing multiple V319C subunits (Fig. 3*F*). Maximum inhibition requires the presence of all four pairs of V319C and E321 (Fig. 3*E1*). Large variation of Cd^{2+} inhibition was observed in channels containing two V319C subunits (Fig. 3*F*), with inhibition in some channels (Fig. 3*E3*) comparable to those containing three V319C subunits (Fig. 3*E2*) and inhibition in others (Fig. 3*E4*, comparable to those containing only one V319C subunit (Fig. 3*E5*); this suggests that the V319C-Cd^{2+}-E321 coordination may also depend on whether coordinating subunits are adjacent to or across from each other. Interestingly, the Hill coefficient of inhibition induced by V319C-Cd^{2+}-E321 coordination is greater than 1 (Fig. 2*D* and Fig. S5), suggesting that binding of multiple Cd^{2+} ions can contribute to inhibition.

Taken together, the above results reveal that V319C and E321 must be in the same BK subunit to form a Cd^{2+} coordination site. The average bond length of Cd^{2+}-Glu(Oδ,Oε) and Cd^{2+}-Cys(S) in a Cd^{2+} coordination site is ∼2.5 Å (20). Therefore, the distance between V319C side chain thiol and E321 side chain carboxyl in a BK subunit should be ∼5 Å. In Kv channel structures (5, 23), the distance between the side chains of equivalent residues (V406 and V408) is more than 10 Å. In addition, V406 and V408 are in not on the same surface of Kv S6 helix because this distance goes through the middle of the helix in Kv channel structure. Therefore, we propose that the conserved proline (P320) in the BK YVP motif may produce a kink in BK S6 that is sharper than that observed in Kv channel structures.

State Dependence of Cd^{2+} Coordination with BK Inner Pore Cysteines. In Kv channels, voltage-dependent gating involves a large conformational change in the C terminus of S6 around the PVP motif, which changes either the structure of Kv inner pore Cd^{2+} coordination sites or accessibility to these sites (24). As a result, Cd^{2+} coordination with cysteines placed in the Shaker inner pore is strongly state-dependent (2–4). To gain insight into conformational changes in the BK inner-pore region during gating, we determined Cd^{2+} coordination rates for V319C or A316C under conditions favoring either open or closed states.

To determine the rate of Cd^{2+}-V319C coordination in open states, channels were held at +100 mV with Po estimated from the *G–V* curve to be ∼0.7 and Cd^{2+} then applied. The time course of inhibition induced by 100 μM Cd^{2+} was fit by a single exponential function with a time constant of 390 ms (Fig. 4*A*). The inhibition time constants were determined in 50, 100, and 200 μM Cd^{2+}. The reciprocal time constants were plotted against $[Cd^{2+}]_{in}$ and fit linearly to determine the second-order rate of Cd^{2+}-V319C coordination in open states (2.8×10^4 $M^{-1}{\cdot}s^{-1}$; Fig. 4*C*). Closed-state coordination was examined at −120 mV during Cd^{2+} application. Brief test steps (160 mV, 2 ms) were applied every 200 ms to monitor residual outward current. Because the duration of these test steps was much shorter than the inhibition time constant in open states, it is therefore unlikely that the apparent closed-state coordination rate was biased by some open-state inhibition occurring during the brief test steps. In accordance with this, the inhibition time course generated by a protocol using 40-ms test steps was identical to that by 2-ms steps (Fig. 4*B*). The closed-state coordination rate of Cd^{2+} with V319C determined from inhibition time constants measured in 50, 100, and 200 μM Cd^{2+} was 2.1×10^4 $M^{-1}{\cdot}s^{-1}$ (Fig. 4*C*), similar to that observed in open states. In contrast, the closed-state coordination of Cd^{2+} with Shaker V474C (equivalent to V319C) is more than 1,000-fold slower than that in open state (Fig. S7). The weak state dependence of the onset of Cd^{2+}-V319C coordination suggests that this site is readily accessible to intracellular Cd^{2+} in both closed and open states.

By a similar strategy, we also examined the state dependence of Cd^{2+}-A316C coordination. The open-state coordination rate determined from inhibition time constants measured in 50, 100, and 200 μM Cd^{2+} at +100 mV was 3.3×10^5 $M^{-1}{\cdot}s^{-1}$ (Fig. 4 *D* and *F*), also comparable to the open state Cd^{2+}-V474C coordination rate observed in Shaker channels (2). To determine the rate of Cd^{2+}-A316C coordination in closed states, inside-out patches containing hundreds of BK A316C channels were held at −120 mV. BK channels were activated by addition of 100 μM Cd^{2+} with a single exponential time constant of 156 ms (Fig. 4*E*). The closed-state Cd^{2+}-A316C coordination rate determined from activation time constants measured in 50, 100, and 200 μM Cd^{2+} is 4.1×10^4 $M^{-1}{\cdot}s^{-1}$ (Fig. 4*F*). The rate of the Cd^{2+}-induced increase in current may reflect both Cd^{2+} coordination and channel gating kinetics, such that the observed rate may be a lower limit of the actual coordination rate. However, conditions favoring BK channel opening only increase the accessibility of A316C to intracellular Cd^{2+} by less than 10-fold. In contrast, for the same patch (Fig. 4 *D* and *E*), the BK channel Po estimated from currents recorded in control solution was increased from 10^{-5} to 0.35 by stepping from −120 to +100 mV, suggesting a concomitant K^+ permeability increase of more than 30,000-fold.

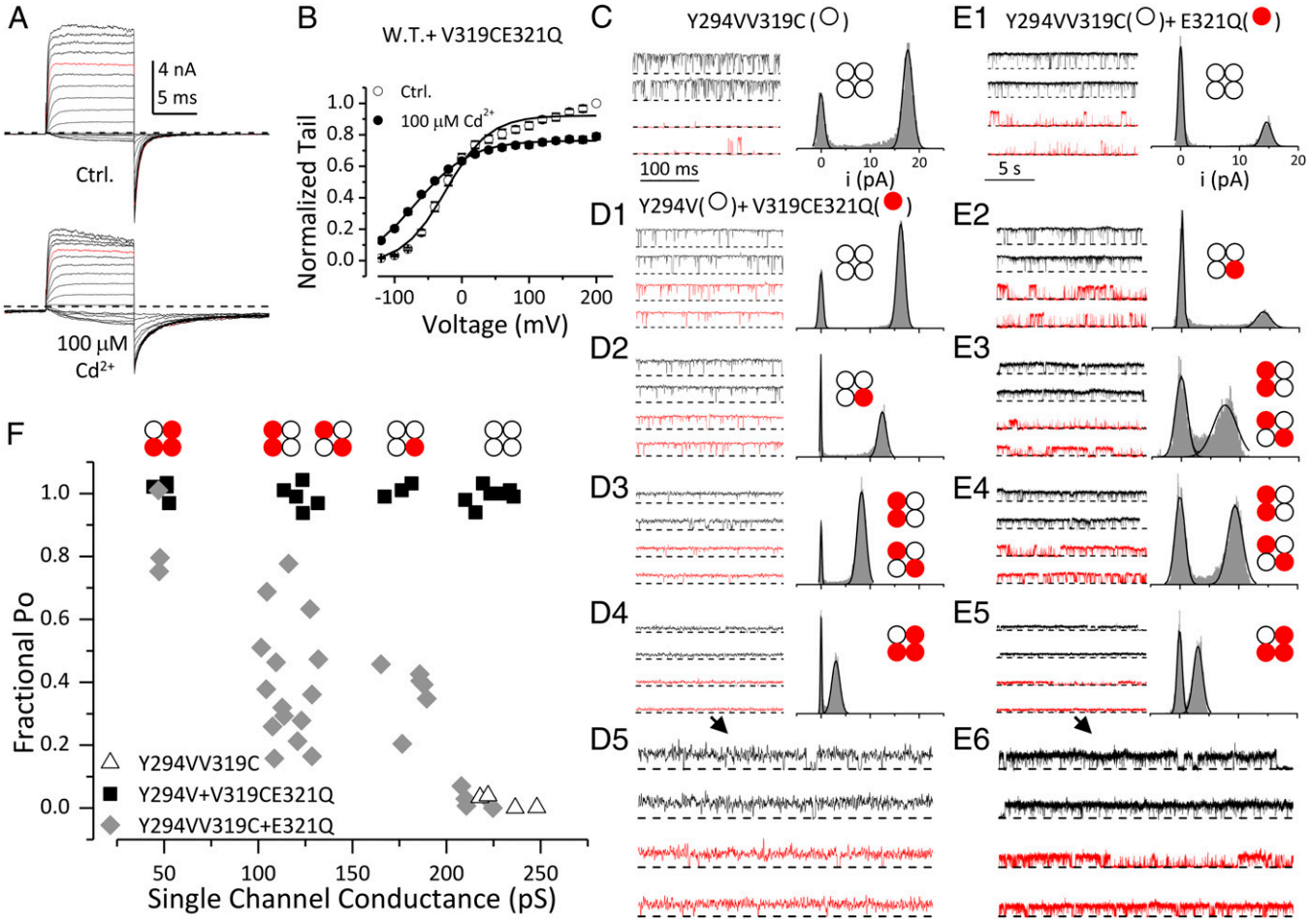

Fig. 3. Cd^{2+} coordinates with V319C and E321 from the same subunit. (*A*) Macroscopic BK currents recorded from oocytes coinjected with WT and V319CE321Q RNAs without (*Upper*) and with (*Lower*) 100 μM intracellular Cd^{2+}. Voltage protocol was the same as in Fig. 1. (*B*) *G–V* relationships of WT + V319CE321Q in 300 μM Ca^{2+} without (open symbols) and with (filled symbols) 100 μM Cd^{2+}. Boltzmann fit results (line) are $z = 0.9e$, $V_h = -23$ mV (control); $z = 0.6e$, $V_h = -68$ mV (Cd^{2+}). (*C–E*) Representative single-channel currents of homomeric and heteromeric BK channels recorded in 300 μM Ca^{2+} at +70 mV without (black) and with (red) 100 μM Cd^{2+}. Closed-channel level is indicated by dotted lines. All-point amplitude histogram on the right of each pair of sample traces was generated from recording in 4 μM Ca^{2+} from the same patch. (*Insets*) Stoichiometry for channel deduced from the single-channel current amplitude. The time scale in *E1–E5* (5 s) is different from that in *C* and *D1–D4* (100 ms). The single-channel traces in *D4* and *E5* are magnified (2×) and displayed in *D5* and *E6*, respectively. (*C*) Single-channel activity of homomeric Y294VV319C channel. (*D1–D5*) Single-channel recordings for the four levels of observed currents recorded from oocytes coinjected with Y294V and V319CE321Q. (*E1–E6*) Single-channel recordings for the four levels of observed currents recorded from oocytes coinjected with Y294VV319C and E321Q. Notice that examples in *E3* and *E4* have similar single-channel conductance but distinct Cd^{2+} sensitivity. (*F*) The fraction of BK Po in 100 μM Cd^{2+} (Po_{Cd}/Po_{Ctrl}) is plotted against single-channel conductance of channels formed by Y294VV319C alone (triangle), coinjection of Y294V and V319CE321Q (square), and coinjection of Y294VV319C and E321Q (diamond). Po was determined from steady-state recordings of 5- to 10-s (Y294VV319C and Y294V + V319CE321Q) or 30- to 90-s (Y294VV319C + E321Q) duration.

A316C is a pore-lining residue positioned a full helical turn extracellularly to the S6 positions that align with those in the Kv channel bundle crossing (Fig. 1*B*), which participate in the restriction to permeant ion flow in closed Kv channels (2). Therefore, the observation that intracellular Cd^{2+} accesses A316C with only a modest state dependence clearly shows that the cytosolic side of a closed BK channel does not significantly restrict access of permeant ions to the inner cavity. Our previous study suggested that the narrowest part of BK inner pore is at the level of A316 (12). Therefore, the current result adds to the evidence suggesting that the selectivity filter is the most likely region to gate ion permeation in BK channels (11, 12, 18, 25, 26). Interestingly, the modest state dependence of A316C-Cd^{2+} coordination is comparable to that observed at an inner pore location in the cyclic nucleotide gated channels (Fig. S7), for which ion permeation is thought to be primarily gated in the selectivity filter region (27).

Discussion

In this study we probed the consequences of Cd^{2+} coordination with cysteines introduced into the BK inner pore region. Our results define two interesting features of BK structure and function in this region. First, Cd^{2+} forms intrasubunit coordination with V319C and E321 in the C terminus of BK S6 with weak state-dependence, suggesting that the conserved proline (P320) between V319C and E321 produces a stable structural feature that differs from the PVP kink observed in Kv channel structures. Second, intracellular Cd^{2+} coordinates with inner pore lining cysteines (A316C) with only modest state dependence, further supporting the idea that the cytosolic side of a closed BK channel does not occlude access of permeant ions to the inner cavity.

Is there any precedence for bends analogous to the proposed BK VPE triplet in known protein structures? Recently, it was shown that two Cd^{2+} binding residues separated by just one residue can form a high-affinity (apparent affinity $K_d < 30$ μM) Cd^{2+} coordination site when they are placed in a β-turn but not

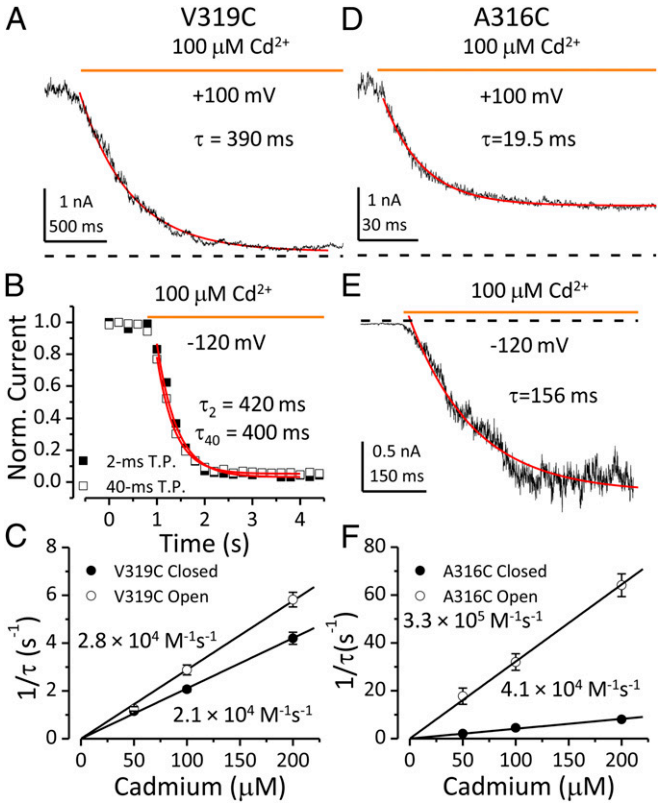

Fig. 4. State-dependent accessibility of BK inner-pore cysteines to intracellular Cd^{2+}. Time courses of current change induced by 100 μM Cd^{2+} are fit by a single exponential function in *A*, *B*, *D*, and *E* (red lines) (*A*) Decay of outward current induced by open state Cd^{2+}-V319C coordination at +100 mV. Zero current level is indicated by dotted line in this panel and in *D* and *E*. (*B*) Inhibition of outward current induced closed-state Cd^{2+}-V319C coordination at −120 mV. Inhibition time courses obtained using 2-ms (filled square) and 40-ms test steps (open square) were identical. (*C*) Reciprocal time constants of Cd^{2+}-V319C coordination in open (open circle) or closed (filled circle) states plotted against $[Cd^{2+}]_{in}$. The second-order rate constant of Cd^{2+} coordination is determined from the slope of a linear fit (line). (*D*) Decay of outward current induced by open-state Cd^{2+}-A316C coordination at +100 mV. (*E*) Increase of inward current induced by closed-state Cd^{2+}-A316C coordination at −120 mV. (*F*) Reciprocal time constants of Cd^{2+}-A316C coordination in open (open circle) and closed (filled circle) states are plotted against $[Cd^{2+}]_{in}$ to determine second-order rate constants of Cd^{2+}-A316C coordination by a linear fit (line).

in an α-helix (19). In addition to breaks or kinks in α-helices, proline is also frequently found in β-turns (28), with two residues adjacent to proline close enough to allow Cd^{2+} coordination. In such structures, proline is often followed by an acidic residue (29–32). For example, the distance between I64-Cβ and E66-Cδ in a triplet sequence IPE found in a β-turn of the gene 3 protein structure is ∼6 Å, which is permissive for Cd^{2+} coordination (29). In the structure of *Sulfolobus shibatae* isopentenyl diphosphate isomerase, the distance between V265-Cβ and D267-Cβ in a triplet sequence VPD is also less than 6 Å (30). Interestingly, the side chain oxygen and the backbone amino group of the acidic residue in such triplets are usually close enough (3 Å or less) to form an intraresidue hydrogen bond. Fig. 5 and Fig. S8 show a structural model of the BK PGD (orange in Fig. 5) using the Kv1.2 structure (PDB ID code 2A79, blue) as an initial template. Taking into account both our previous (12) and the current functional results, we adjusted dihedral angles in the double-glycine hinge to orient the side chains of three BK pore-lining residues (A313, A316, S317, green) into the central pore. Dihedral angles in the VPE triplet were then adjusted to match those found in the IPE triplet of the gene 3 protein structure (PDB ID code 3KNQ). These structural manipulations reduce the distance between the side chains of V319C and E321 from 10.3 to 5.1 Å, which is ideal for Cd^{2+} coordination. In this hypothetical structure, the conserved proline in the BK YVP motif produces a curvature more marked than that observed in the Kv1.2 structure. Such a structural feature would be likely to alter the points of contact between S6 and S4–S5 linker, if the BK S4–S5 linker adopted a similar arrangement as that observed in Kv channel structures.

At present, we cannot completely rule out the possibility that the proposed β-turn structure of the BK VPE triplet is induced by intracellular Cd^{2+}. Such a possibility would require the BK S6 to be unusually flexible around P320, which seems unlikely for several reasons. First, based on limited MTSET accessibility, V319C appears to be partially buried in both open and closed states (12); second, P320 would be expected to impose rigid constraints on backbone rotation due to its cyclic five-member ring structure (33); and third, E321 may also limit backbone rotation because of the potential for glutamate to form a hydrogen bond between its side chain oxygen and a backbone amino group (29, 30). Finally, that the onset of Cd^{2+} inhibition (as reported by brief depolarizing steps) is similar both when measured at −120 mV (low Po) and +120 mV (high Po) (Fig. 4 *A*–*C*) also supports the idea that the availability of residues involved in Cd^{2+} coordination are minimally influenced by channel conformational status. For these reasons, we prefer the view that the β-turn structure revealed by Cd^{2+} is an intrinsic part of native VPE triplet.

The present results provide strong support for a novel structural feature within BK S6, but do not answer the question of how Cd^{2+} produces inhibition by coordination between V319C and E321. BK V319 is equivalent to Shaker V474, the valine in the Kv PVP motif. In Shaker V474C construct, a single Cd^{2+} is thought to coordinate with multiple 474 cysteines at the center of the ion permeation pathway to block Kv current by a simple occlusion mechanism (3). In BK V319C, a single-site occlusion model seems unlikely. Although binding of a single Cd^{2+} is sufficient to produce some inhibition of channels containing only a single V319CE321 subunit (Fig. 3*E5*), the concentration dependence of Cd^{2+} inhibition for V319C revealed a Hill coefficient of ∼2 (Fig. S5), suggesting that multiple Cd^{2+} ions participate in inhibition. Furthermore, the ability of bulky MTS

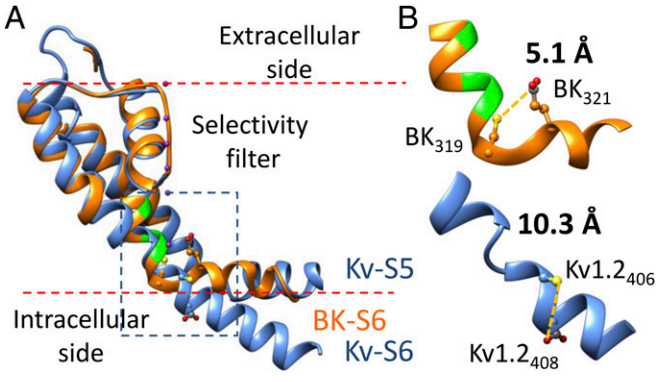

Fig. 5. A hypothetic structure of the BK PGD based on the Kv1.2 crystal structure and functional results from our previous and current studies. (*A*) The hypothetic structure of BK PGD (orange) is superimposed with the Kv1.2 structure (blue). Three pore-lining residues of BK channel (A313, A316, and S317) are colored in green. The S5 of the BK structure is omitted for clarity. K^+ ions are rendered as purple balls. Lipid membrane is delimited by red dotted lines. The boxed region is magnified in *B* to show the structure around the YVP/PVP motif. Side chains of BK_{319}, BK_{321}, $Kv1.2_{406}$, and $Kv1.2_{408}$ (equivalent to $Shaker_{474}$ and $Shaker_{476}$) are rendered as ball and chain. Notice that $Kv1.2_{406}$ and $Kv1.2_{408}$ are not on the same surface of the Kv S6 helix.

PHYSIOLOGY

reagent to modify residues deeper within the inner pore than V319C suggests that the aperture at the level of V319C would be unlikely to be occluded by a single Cd^{2+}ion (12). Therefore, the mechanism of Cd^{2+}-dependent inhibition observed in BK V319C is likely to be different from that proposed for Shaker V474C.

In summary, we have probed two Cd^{2+} coordinating positions in BK S6 to make inferences about structure and function of this part of the channel. The state dependence of Cd^{2+} coordination at both sites is not strong, arguing against an ion permeation gate at the cytosolic end of S6 in BK channels. In addition, Cd^{2+} coordination with a substitution cysteine in this region (V319C) required a native glutamate (E321) from the same subunit. Based on the Kv1.2 structure, this distance between the side chains of residues in register with V319 and E321 should be too far to form an intrasubunit Cd^{2+} coordination site, which strongly suggests a significant structural difference between BK and Kv S6 at a position that may play critical functional roles in coupling VSD movement to S6 motions. Such structural differences may contribute to the functional differences between BK and Kv channels, such as the relatively weak coupling observed between VSD movement and PGD gating in BK channels (34, 35).

Materials and Methods

Mutagenesis and Channel Expression. The background channel contains the C430S mutation to eliminate sensitivity to MTSET (36); it is referred to as WT channel in this study. Mutants were prepared as described before (14). BK channels were expressed in stage IV *Xenopus* oocytes following cRNA injection.

Electrophysiology and Data Analysis. Currents were recorded from inside-out patches (37) with an Axopatch 200B amplifier (Molecular Devices). Macroscopic currents and single-channel currents were low-pass filtered with the integral four-pole Bessel filter at 10 and 2 kHz, respectively. Signals were digitized with Digidata 1322A data acquisition system (Molecular Devices) at 100 kHz. The recordings were controlled by the pClamp 9.2 software suite (Molecular Devices). All experiments were performed at room temperature (21–24 °C).

Recording electrodes were filled with pipette solution containing (in mM): 140 potassium methanesulfonate (KMES), 20 KOH, 10 Hepes, 2 $MgCl_2$ (pH 7.0). Cd^{2+} and other reagents were applied onto patches through bath solution using an SF-77B fast perfusion stepper system (Warner Instruments). The solution changing speed of this system is less than 5 ms, measured from open tip response. Activation time constant of BK current by switching from 0 to 100 μM Ca^{2+} is less than 20 ms at +80 mV. The standard bath solution (cytosolic side of inside-out patch) contained (in mM): 140 KMES, 20 KOH, 10 Hepes (pH 7.0). Solutions with various [Ca^{2+}] (0, 4, and 300 μM) were prepared as described before (17, 38). For experiments using MTSET, aliquots of 100-mM stock solution were thawed and diluted to the desired concentration in bath solution immediately before application. MTSET was obtained from Toronto Research Chemicals. 1N KOH solution was obtained from Fisher Scientific. All other chemicals were purchased from Sigma-Aldrich.

Data analysis and molecular modeling are described in *SI Materials and Methods*.

ACKNOWLEDGMENTS. We thank Drs. Borna Ghosh and Vivian Gonzalez-Perez for insightful comments. This work was supported by NIH Grant GM066215 (to C.J.L.).

1. Hille B (2001) *Ion Channels of Excitable Membranes* (Sinauer, Sunderland, MA), 3rd Ed.
2. del Camino D, Yellen G (2001) Tight steric closure at the intracellular activation gate of a voltage-gated K(+) channel. *Neuron* 32(4):649–656.
3. Liu Y, Holmgren M, Jurman ME, Yellen G (1997) Gated access to the pore of a voltage-dependent K+ channel. *Neuron* 19(1):175–184.
4. Webster SM, Del Camino D, Dekker JP, Yellen G (2004) Intracellular gate opening in Shaker K+ channels defined by high-affinity metal bridges. *Nature* 428(6985): 864–868.
5. Long SB, Campbell EB, Mackinnon R (2005) Crystal structure of a mammalian voltage-dependent Shaker family K+ channel. *Science* 309(5736):897–903.
6. Long SB, Campbell EB, Mackinnon R (2005) Voltage sensor of Kv1.2: Structural basis of electromechanical coupling. *Science* 309(5736):903–908.
7. Lu Z, Klem AM, Ramu Y (2001) Ion conduction pore is conserved among potassium channels. *Nature* 413(6858):809–813.
8. Lu Z, Klem AM, Ramu Y (2002) Coupling between voltage sensors and activation gate in voltage-gated K+ channels. *J Gen Physiol* 120(5):663–676.
9. Salkoff L, Butler A, Ferreira G, Santi C, Wei A (2006) High-conductance potassium channels of the SLO family. *Nat Rev Neurosci* 7(12):921–931.
10. Tang QY, Zeng XH, Lingle CJ (2009) Closed-channel block of BK potassium channels by bbTBA requires partial activation. *J Gen Physiol* 134(5):409–436.
11. Wilkens CM, Aldrich RW (2006) State-independent block of BK channels by an intracellular quaternary ammonium. *J Gen Physiol* 128(3):347–364.
12. Zhou Y, Xia XM, Lingle CJ (2011) Cysteine scanning and modification reveal major differences between BK channels and Kv channels in the inner pore region. *Proc Natl Acad Sci USA* 108(29):12161–12166.
13. Li W, Aldrich RW (2006) State-dependent block of BK channels by synthesized shaker ball peptides. *J Gen Physiol* 128(4):423–441.
14. Xia XM, Zeng X, Lingle CJ (2002) Multiple regulatory sites in large-conductance calcium-activated potassium channels. *Nature* 418(6900):880–884.
15. Zeng XH, Xia XM, Lingle CJ (2005) Divalent cation sensitivity of BK channel activation supports the existence of three distinct binding sites. *J Gen Physiol* 125(3):273–286.
16. Shi J, et al. (2002) Mechanism of magnesium activation of calcium-activated potassium channels. *Nature* 418(6900):876–880.
17. Zhang X, Solaro CR, Lingle CJ (2001) Allosteric regulation of BK channel gating by Ca(2+) and Mg(2+) through a nonselective, low affinity divalent cation site. *J Gen Physiol* 118(5):607–636.
18. Chen X, Yan J, Aldrich RW (2014) BK channel opening involves side-chain reorientation of multiple deep-pore residues. *Proc Natl Acad Sci USA* 111(1):E79–E88.
19. Puljung MC, Zagotta WN (2011) Labeling of specific cysteines in proteins using reversible metal protection. *Biophys J* 100(10):2513–2521.
20. Rulísek L, Vondrásek J (1998) Coordination geometries of selected transition metal ions (Co2+, Ni2+, Cu2+, Zn2+, Cd2+, and Hg2+) in metalloproteins. *J Inorg Biochem* 71(3-4):115–127.
21. Shen KZ, et al. (1994) Tetraethylammonium block of Slowpoke calcium-activated potassium channels expressed in Xenopus oocytes: Evidence for tetrameric channel formation. *Pflugers Arch* 426(5):440–445.
22. Niu X, Magleby KL (2002) Stepwise contribution of each subunit to the cooperative activation of BK channels by Ca2+. *Proc Natl Acad Sci USA* 99(17):11441–11446.
23. Long SB, Tao X, Campbell EB, MacKinnon R (2007) Atomic structure of a voltage-dependent K+ channel in a lipid membrane-like environment. *Nature* 450(7168): 376–382.
24. Bezanilla F (2008) How membrane proteins sense voltage. *Nat Rev Mol Cell Biol* 9(4): 323–332.
25. Chen X, Aldrich RW (2011) Charge substitution for a deep-pore residue reveals structural dynamics during BK channel gating. *J Gen Physiol* 138(2):137–154.
26. Thompson J, Begenisich T (2012) Selectivity filter gating in large-conductance Ca(2+)-activated K+ channels. *J Gen Physiol* 139(3):235–244.
27. Contreras JE, Srikumar D, Holmgren M (2008) Gating at the selectivity filter in cyclic nucleotide-gated channels. *Proc Natl Acad Sci USA* 105(9):3310–3314.
28. Hutchinson EG, Thornton JM (1994) A revised set of potentials for beta-turn formation in proteins. *Protein Sci* 3(12):2207–2216.
29. Jakob RP, et al. (2010) Elimination of a cis-proline-containing loop and turn optimization stabilizes a protein and accelerates its folding. *J Mol Biol* 399(2):331–346.
30. Unno H, et al. (2009) New role of flavin as a general acid-base catalyst with no redox function in type 2 isopentenyl-diphosphate isomerase. *J Biol Chem* 284(14):9160–9167.
31. Hosfield DJ, et al. (2004) Structural basis for bisphosphonate-mediated inhibition of isoprenoid biosynthesis. *J Biol Chem* 279(10):8526–8529.
32. Eckhardt B, Grosse W, Essen LO, Geyer A (2010) Structural characterization of a beta-turn mimic within a protein-protein interface. *Proc Natl Acad Sci USA* 107(43): 18336–18341.
33. Creighton TE (1992) *Proteins: Structures and Molecular Properties* (Freeman, New York), 2nd Ed.
34. Horrigan FT, Aldrich RW (2002) Coupling between voltage sensor activation, Ca2+ binding and channel opening in large conductance (BK) potassium channels. *J Gen Physiol* 120(3):267–305.
35. Horrigan FT, Cui J, Aldrich RW (1999) Allosteric voltage gating of potassium channels I. Mslo ionic currents in the absence of Ca(2+). *J Gen Physiol* 114(2):277–304.
36. Zhang G, Horrigan FT (2005) Cysteine modification alters voltage- and Ca(2+)-dependent gating of large conductance (BK) potassium channels. *J Gen Physiol* 125(2):213–236.
37. Hamill OP, Marty A, Neher E, Sakmann B, Sigworth FJ (1981) Improved patch-clamp techniques for high-resolution current recording from cells and cell-free membrane patches. *Pflugers Arch* 391(2):85–100.
38. Zeng XH, Ding JP, Xia XM, Lingle CJ (2001) Gating properties conferred on BK channels by the beta3b auxiliary subunit in the absence of its NH(2)- and COOH termini. *J Gen Physiol* 117(6):607–628.